EARTH SURFACE PROCESSES AND LANDFORMS
Earth Surf. Process. Landforms **37**, 262–272 (2012)

Published online 4 October 2011 in Wiley Online Library
(wileyonlinelibrary.com) DOI: 10.1002/esp.2234

Multitemporal ALSM change detection, sediment delivery, and process mapping at an active earthflow

Stephen B. DeLong,[1,2]* Carol S. Prentice,[2] George E. Hilley[3] and Yael Ebert[3]
[1] Biosphere 2, University of Arizona, Tucson, AZ, USA
[2] MS 977 US Geological Survey, Menlo Park, CA, USA
[3] Stanford University, Stanford, CA, USA

Received 23 November 2010; Revised 31 August 2011; Accepted 5 September 2011

*Correspondence to: Stephen B. DeLong, Biosphere 2, University of Arizona, PO Box 8746, Tucson, AZ 85738, USA. E-mail: sdelong@email.arizona.edu

ESPL
Earth Surface Processes and Landforms

ABSTRACT: Remote mapping and measurement of surface processes at high spatial resolution is among the frontiers in Earth surface process research. Remote measurements that allow meter-scale mapping of landforms and quantification of landscape change can revolutionize the study of landscape evolution on human timescales. At Mill Gulch in northern California, USA, an active earthflow was surveyed in 2003 and 2007 by airborne laser swath mapping (ALSM), enabling meter-scale quantification of landscape change. We calculate four-year volumetric flux from the earthflow and compare it to long-term catchment average erosion rates from cosmogenic radionuclide inventories from adjacent watersheds. We also present detailed maps of changing features on the earthflow, from which we can derive velocity estimates and infer dominant process. These measurements rely on proper digital elevation model (DEM) generation and a simple surface-matching technique to align the multitemporal data in a manner that eliminates systematic error in either dataset. The mean surface elevation of the earthflow and an opposite slope that was directly influenced by the earthflow decreased 14 ± 1 mm/yr from 2003 to 2007. By making the conservative assumption that these features were the dominant contributor of sediment flux from the entire Mill Gulch drainage basin during this time interval, we calculate a minimum catchment-averaged erosion rate of $0{\cdot}30 \pm 0{\cdot}02$ mm/yr. Analysis of beryllium-10 (^{10}Be) concentrations in fluvial sand from nearby Russian Gulch and the South Fork Gualala River provide catchment averaged erosion rates of $0{\cdot}21 \pm 0{\cdot}04$ and $0{\cdot}23 \pm 0{\cdot}03$ mm/yr respectively. From translated landscape features, we can infer surface velocities ranging from 0·5 m/yr in the wide upper 'source' portion of the flow to 5 m/yr in the narrow middle 'transport' portion of the flow. This study re-affirms the importance of mass wasting processes in the sediment budgets of uplifting weak lithologies. Copyright © 2011 John Wiley & Sons, Ltd.

KEYWORDS: LiDAR; hillslope; morphological sediment budgeting; DEM differencing; mass wasting

Introduction

Earthflows can be an important, and in some places, dominant, phenomena in steep mountainous regions underlain by weak fine-grained lithologies. One such region is the steep and rising Coast Ranges of California, much of which are underlain by weak, argillaceous Franciscan Complex. Mackey and Roering (2011) recently provided a detailed review of earthflow process on Franciscan bedrock in northern California. They describe short-term earthflow behavior that involves intermittent motion followed by periods of dormancy. This short-term behavior is largely controlled by soil moisture and groundwater levels because earthflows tend to move when elevated pore water pressure leads to movement on transient slide planes (Kelsey, 1978; Keefer and Johnson, 1983; Iverson and Major, 1987). Mackey and Roering (2011) also propose a long-term model for earthflow behavior that includes periods of activity on a hundred-year timescale followed by much longer periods of dormancy. They suggest the timing and rates of these cycles are modulated by local channel base-level lowering and upstream source area availability. Sediment delivery from earthflows can account for a significant portion (perhaps up to 50%) of a catchment sediment budget in locations underlain by extensive weak, fine-grained, even where earthflows are formed on less than 10% of the watershed area (Kelsey, 1978; Mackey and Roering, 2011). As such, improved methods for quantification of mass movement sediment delivery are required to better understand landscape evolution in highly erosive landscapes.

Because earthflows are active on human timescales and can make up a considerable fraction of the landscape in fine-grained lithologies [6% of the Eel River study area was reported to be active earthflow in Mackey and Roering (2011)], they are important agents of landscape change. The frequent (generally at least seasonal, if not continuous) movement of active earthflows also provides an opportunity to refine techniques for remote, high resolution landscape change analysis on fairly short timescales. Such accurate, high resolution, and quantitative three-dimensional measurements of landscape change from remote airborne and/or satellite platforms represent a frontier in Earth surface process research (Merritts *et al.*, 2008,

Tarolli *et al.*, 2009). High resolution topographic data gathered from airborne laser swath mapping (ALSM) (also referred to as airborne light detection and ranging or LiDAR) can provide detailed post-event topographic change detection over large spatial extents if pre-event data are available, and can also quantify rates of continuous and intermittent landscape change not related to particular events. Repeat ALSM can be used to detect changes that may be too subtle for detection by other methods or detect change in remote areas that would otherwise go unnoticed. We were partially motivated to analyze active change at an earthflow by the anticipated need to use disparate ALSM datasets when undertaking rapid post-event (earthquakes and storms, in particular) landscape change and damage assessment. We were also interested in the application of repeat ASLM campaigns in order to establish direct, high accuracy measurement of volumetric flux at the scale of drainage basins in some rapidly eroding, low vegetation landscapes. Direct, remote measurement of catchment sediment flux would be a powerful tool in studies of landscape development. Furthermore, like Mackey and Roering (2011), we were motivated to better understand the rates and style of earthflow processes in remote areas, and over large spatial scales.

Multitemporal ALSM has been used across a range of geomorphic settings. It is particularly well established in coastal environments because coastal changes are frequent, and multitemporal data have been collected in many locations (e.g. Woolard and Colby, 2002; Lazarus and Murray, 2007; Houser *et al.*, 2008; Pelletier *et al.*, 2009; Mitasova *et al.*, 2009; Zhou and Xie, 2009). Fluvial change detection using high resolution topography has recently been refined to the point it is now a reliable quantitative method (Wheaton *et al.*, 2010). Jaboyedoff *et al.* (2010) present a detailed review of the use of ALSM and terrestrial laser scanning in landslide research and point out the paucity of published studies that report on the use of ALSM for landslide monitoring. Previous efforts at topographic change detection over large areas in landslide terrains have used interferometric techniques such as InSAR which can provide submeter vertical change detection, but over coarse horizontal scales (e.g. Hilley *et al.*, 2004; Strozzi *et al.*, 2005; Bulmer *et al.*, 2006; Delacourt *et al.*, 2007); aerial photograph analysis and ALSM (Mackey *et al.*, 2009; Mackey and Roering, 2011); InSAR and ALSM (Roering *et al.*, 2009); global positioning system (GPS), theodolite surveys and ALSM (Glenn *et al.*, 2006); and traditional surveying and field observation (Kelsey, 1978; Baum *et al.*, 1998; Coe *et al.*, 2009). Real-time monitoring of point-based velocity fields from survey points on landslides can be accomplished with GPS (Malet *et al.*, 2002). These techniques provide insight into landslide kinematics; however, none provide meter horizontal and sub-meter vertical scale maps of topographic change, nor do any measure volumetric change directly, though Mackey and Roering (2011) estimate sediment delivery from earthflows over a 62 year period using historical aerial photographs and more recent ALSM data to measure surface velocities, and, from that and estimates of cross-sectional area at earthflow toes, calculate an expected volume flux. In what was the seminal study of earthflow sediment delivery, Kelsey (1978) used repeat surveys and historical aerial photograph analysis, and some direct measurements of earthflow thickness to quantify sediment delivery from several earthflows along the Van Duzen River in California. These types of calculations do not take into account the potential for significant thickness changes, nor sediment delivery from surficial gully systems, nor do they map landscape change in the vertical dimension. The surface velocity of an earthflow at the toe can only be used to calculate sediment yield only if there is no topographic change (thickening or thinning) at the earthflow toe. The considerable length of their analysis (62 years) serves to minimize this effect, but their study nonetheless provides motivation for an approach to change detection using multitemporal ALSM in three dimensions, which we provide here.

Change detection in landslide terrains in Italy using multitemporal ALSM data collected from helicopter platforms led to development of maps of change that highlighted meter-scale vertical topographic changes (Corsini *et al.*, 2007; Corsini *et al.*, 2009). These studies also reported volumetric changes in two large landslide complexes, and present a useful precedent for the present study.

Perhaps the most comprehensive analysis to date of the use of multitemporal ALSM in landslide terrains is Burns *et al.* (2010). They compared ALSM data collected by the same technology in September and December 2007 in heavily forested terrain. Their careful analysis largely addressed error in and sensitivity of ALSM collection, and they highlighted the challenges of ALSM collection in 'leaf-on' conditions in forested terrains that lead to extensive elevation interpolation when a gridded digital elevation model (DEM) is made from laser returns classified as ground. They conclude that, in the challenging setting that they worked, subtle landslide changes were not particularly easy to identify, but that multitemporal ALSM collection in 'leaf-off' conditions might hold more promise. They make volumetric estimates of change between scans, but suggest that they are not able to distinguish errors in data from actual landscape change with great confidence.

A particularly detailed approach to landslide monitoring was presented by Baldo *et al.* (2009) using multitemporal terrestrial laser scanner data. Their techniques provide impressive three-dimensional change detection but are particularly labor-intensive and cover an area only approximately 150 m across. Bull *et al.* (2010) report on use of multitemporal ALSM for detailed mapping of debris flow deposits. This detailed study relies on 4 m grid resolution and reports confidence in elevation comparisons at the 0·4 m level. They use these data to calculate the volume of debris flow deposits in their study area. These studies serve as motivation for the larger spatial scale (compared to terrestrial laser scanner) and higher resolution [compared to Bull *et al.*'s (2010) study focused on a debris flow depositional area] analyses of sediment source area landscape change we present here. Further, we were motivated to improve the spatial extent and resolution of remote landslide change mapping and to evaluate the possibility of direct measurement of volumetric flux in hillslope source areas.

Detecting landscape change with multitemporal high-resolution topographic data requires pre- and post-change data and reliable procedures for spatial alignment of both datasets. The scale of landscape features that are resolved by ALSM varies widely due to collection methods (e.g. collection altitude, instrument type), and environmental factors, especially vegetation density. ALSM data are able to resolve meter-scale landforms in areas of low vegetation density, but laser ground returns under heavy canopy often have gaps of up to several to even tens of meters. Care must be taken when comparing meter and sub-meter geospatial data published in different coordinate systems. To address these challenges, two datasets collected over high-relief terrain in northern California in 2003 and 2007 using different ALSM technologies and with different mission specifications and deliverables were analyzed.

Study Site: Mill Gulch, Northern California

A slow-moving earthflow on the flank of Mill Gulch (Figure 1) was imaged in its entirety during ALSM collection in 2003 and 2007. This earthflow consists of fine-grained soil and

Figure 1. Location of study area in northern California. This figure is available in colour online at wileyonlinelibrary.com/journal/espl

weathered bedrock formed in re-activated landslides of Franciscan Coastal Belt sandstone and shale, and flows by sliding on many ephemeral slide planes (Manson *et al.*, 2006). Earthflows in general tend to move episodically after significant precipitation due to increased pore-water pressure (Kelsey, 1978; Iverson and Major, 1987).

The earthflow sits on a south-facing grass-covered slope with a few scattered trees. Just to the north and east, dense redwood forest covers the landscape. The opposite, north-facing slope (a small part of which failed between 2003 and 2007, and so is within the domain of this study) is covered by patchy brush and trees. The earthflow is tightly coupled with the canyon-floor channel at its toe; flow lobes sit directly on the active channel bed. The head of the earthflow has reached a local drainage divide over a portion of its extent, and has a sharp scarp that cuts into a smooth hillslope with a single prominent gully along the rest of its headward extent (visible in Figures 2d and 3).

Methods

Two ALSM datasets, collected by two different instruments were used for this study. These were the 2003 Northern San Andreas Fault ALSM data and 2007 Northern California GeoEarthScope ALSM data. Both of these data sets were primarily collected for investigation of the San Andreas Fault Zone, which is just down-canyon from the Mill Gulch earthflow, but fortunately both were wide enough to image the entirety of the earthflow. A key requirement of this study was to align these disparate data sources in three dimensions. This can be done in two ways: (1) by using a geographic transformation to match coordinate systems or (2) by a surface matching technique using portions of the landscape that are assumed to be unchanged between datasets. Both were evaluated and utilized in this study.

The February 2003 data were collected using an unnamed proprietary laser altimeter by TerraPoint, USA, Inc. The reported horizontal accuracy is 0·5 m and the reported vertical accuracy is 0·15 m. The average laser return density in the study area is between 5–7 returns/m^2. Individual points were classified as blunder, vegetation, ground and buildings using Terrascan software. The average point density of points classified as ground at the earthflow is ~3·0 points/m^2. The data were delivered in the State Plane system (California II Zone), NAD83 datum, with horizontal units of US Survey feet (0·30480061 m) and vertical units of International Feet (0·3048 m) as orthometric heights using the Geoid99 model (TerraPoint and Harding, 2004).

The 2007 NoCAL data were collected using an Optech Gemini airborne laser platform operated by the National Center for Airborne Laser Mapping (NCALM) between March 21, 2007 and April 17, 2007. The reported horizontal accuracy is ≤ 0·36 m, and the reported vertical accuracy was typically 0·05–0·1 m (NCALM, 2007). The average laser return density in the study area is between 16 and 22 returns/m^2. Individual points were classified as low, aerial, ground or non-ground using TerraScan software. The average point density of points classified as ground at the earthflow is ~5·5 points/m^2. These data were released in WGS84(ITRF2000) datum reference frame in Universal Transverse Mercator (zone 10 N) coordinates with vertical units of meters above the ellipsoid. The epoch date of the coordinate system is 2007·25.

In order to prepare ALSM data for change detection, DEMs from classified point cloud data were produced for 2003 and 2007 using identical parameters within online tools available at http://www.opentopography.org. These tools allow the point cloud to be queried in order to create a range of derivative products (Arrowsmith and Zielke, 2009). DEMs were created from ground-classified points using a 2 m search window, an inverse distance weighted (IDW) mean interpolation algorithm, and were gridded to a 1 m resolution raster. This search radius was selected by visual interpretation of gridding results. Lowering this value resulted in more frequent grid points with no elevation data, and increasing it results in greater interpolation distances over areas with no useful elevation data. This procedure produced DEMs that (1) represent bare earth topography well in areas with laser ground returns spaced less than 2 m, and (2) maintain 'no data' holes in areas with sparse (> 2 m apart) ground returns so that any local errors or gaps in ground elevation data are not propagated laterally more than 1–2 m. We specifically avoided long-distance interpolation to fill no data holes in order to avoid analysis of landscape change where no data exists or is highly generalized. Standard NCALM gridded DEM products commonly used by the geologic community are created using a 25 m search window and a kriging

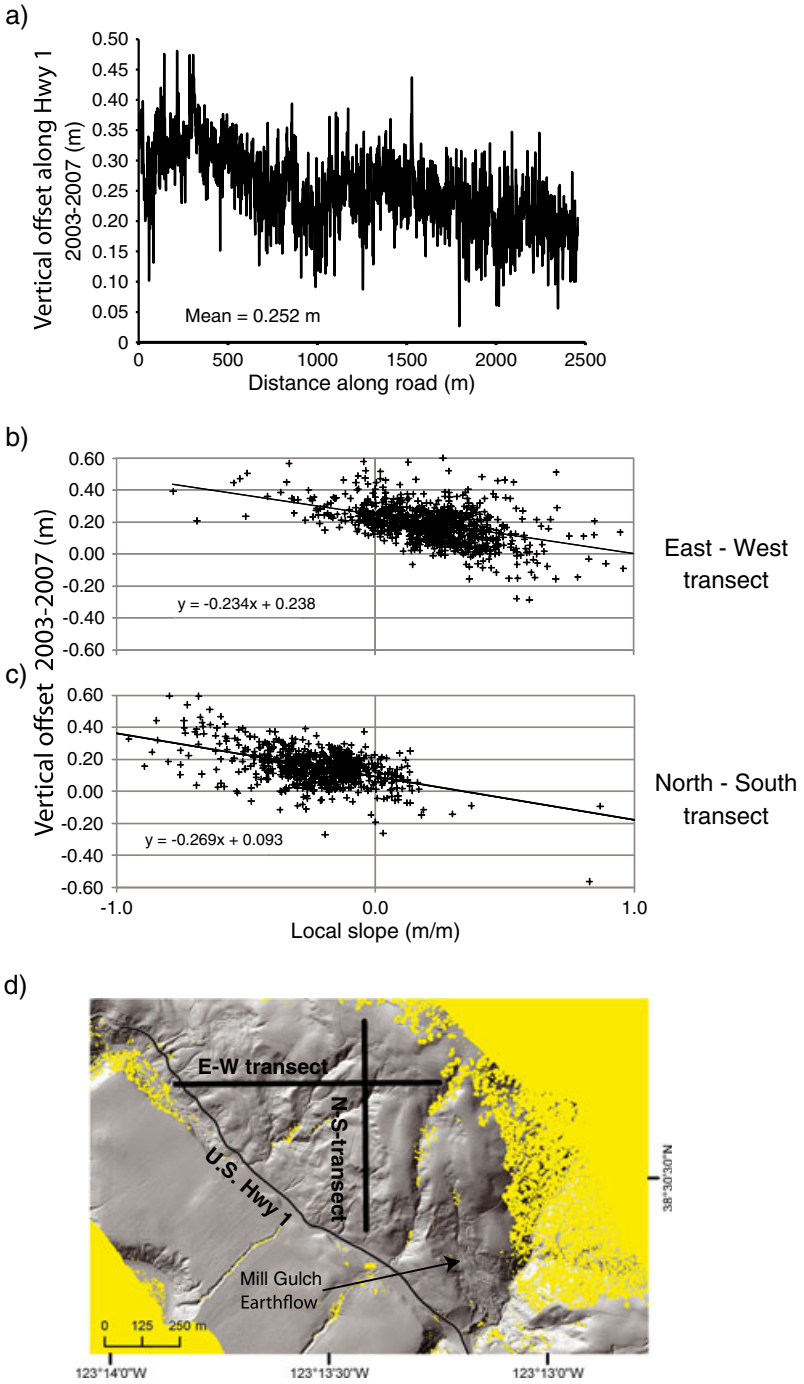

Figure 2. (a). Vertical offset along Highway 1 after geographic transformation-based alignment but before surface-matching alignment. Mean value of 0·25 m was used for vertical offset correction. The variation across this transect indicates that offset is not equally distributed in space. This suggests that local alignment may be necessary and that errors do not appear to be systematic over entire datasets. (b) Vertical offset between 2003 and 2007 data plotted as slope versus vertical offset along an east–west transect. The weak dependence of vertical offset on slope indicates horizontal misalignment. The magnitude of this misalignment is the slope of the trendline (0·23 m). (c) Vertical offset versus local slope for a north–south transect. These data indicate a north–south misalignment of 0·27 m. (d) Locations of transects. Yellow pixels are areas where the DEM generation algorithm did not find ground elevation values within the search radius, and, as such, are 'no data'. After surface matching alignments based on these data, the slope of the relationship between slope and vertical offset for the north–south and east–west trendlines approached zero. The values of R^2 for these data are low (0·15 for east–west and 0·24 for north–south), reflecting the minor nature of the misalignment of inherently noisy data. However, after manual alignment, R^2 values are less than 0·01 in each case. This figure is available in colour online at wileyonlinelibrary.com/journal/espl

interpolation algorithm. These processes eliminate nodata holes in areas with sparse ground returns. This creates impressive terrain visualization, but local elevation values are interpolated over long distances and may not represent true landscape form.

In order to properly align the two ALSM datasets for change detection, gridded elevation data from 2003 were projected into the UTM NAD83 coordinate system. The gridded elevation data from 2007 were transformed from WGS84(ITRF2000)(2007·25) to NAD83 using a 14-parameter Helmert transformation parameters as specified in Soler and Snay (2003) and implemented using Proj.4 open-source cartographic projection tools within GRASS GIS. The data were then converted to orthometric heights using the GEOID99 model to match the 2003 data. These transformations, in principle, should have aligned the two datasets to within vendor-specified error; however, a slight but detectable

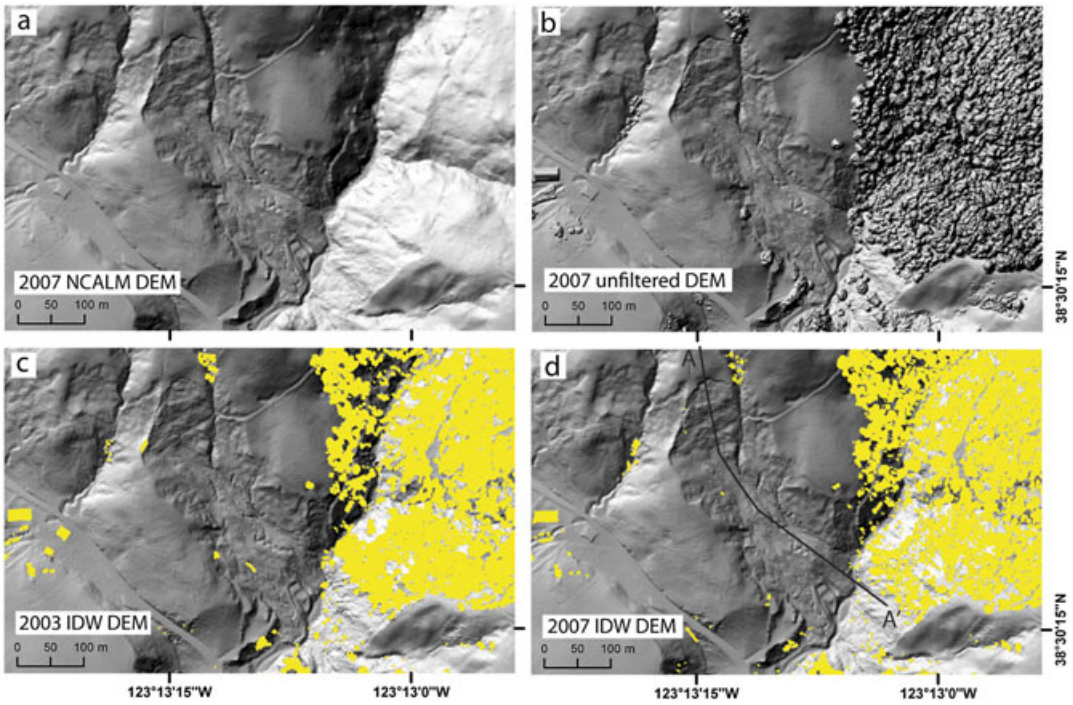

Figure 3. (a) Shaded relief map of 2007 NCALM-processed bare earth DEM. (b) Shaded relief map of unfiltered 2007 NCALM DEM. (c) Shaded relief map of 2 m search radius, 1 m grid spacing IDW DEM from 2003 TerraPoint-processed ground return point cloud. No data in yellow. (d) Shaded relief map of 2 m search radius, 1 m grid spacing IDW DEM from 2007 NCALM-processed ground return point cloud. No data in yellow. A–A' transect for Figure 2 indicated. This figure is available in colour online at wileyonlinelibrary.com/journal/espl

systematic offset remained between the two datasets (the offset was detectable by visual inspection of landscape features, and by the correlation between vertical offset and slope between the datasets). In order to address this, an efficient approach that exploits the systematic variation in vertical offset between two horizontally-misaligned datasets in sloped areas to make *X* and *Y* corrections was used (following Streutker *et al.*, 2011). Systematic vertical offset in flat and unchanged areas (i.e. a paved road and zero-slope areas) was used to make *Z* corrections (Mitasova *et al.*, 2009). Assuming that error in this step is the most appropriate to propagate through to our change analysis, we use the standard error of the mean of the road and flat-area data as the error for our elevation change analysis. Figure 2 illustrates the data and procedures we used for the surface matching approach. The magnitude of these *XYZ* translations were 0·27, 0·23, and 0·25 m respectively, indicating that the coordinate system transformation aligned the data at sub-meter level, but that further decimeter scale misalignment was detectable. We applied these final *XYZ* translations manually. This method has the added benefit of correcting any slight operator errors in executing geographic transformations.

Once the two datasets were aligned, grid subtraction was used to create maps of elevation difference. Wheaton *et al.* (2010) have formalized methods for elevation error estimates for high resolution topographic change detection in fluvial environments based on point density, point quality and local slope. These tools are largely based on knowledge of spatial variability of uncertainty; these are not explicitly known for the data we used, so we took a simple approach to handling uncertainly by conservatively assuming a minimum level of detection of ~0·25 m based on change in areas with little probability of real change (i.e. amplitude of noise in Figure 2a), and the original data specifications.

In order to compare the short-term landscape change rates determined by ALSM change detection with longer-term erosion rates, we analyzed beryllium-10 (^{10}Be) concentrations in fluvial sands deposited along the channel margins of two nearby catchments. We opted not to sample the Mill Gulch catchment itself for ^{10}Be erosion rate determination because of its small size. Larger drainage basins integrate discrete episodes of sediment delivery into a millennial-scale, catchment-averaged erosion rates, especially in steep, high erosion rate catchments (e.g. DiBiase *et al.*, 2010).

Fluvial sands were collected from nearby Russian Gulch and the South Fork Gualala River at Hauser Bridge. Samples were processed to accelerator mass spectrometry (AMS) targets at the Stanford Tectonic Geomorphology Laboratory Cosmogenic Radionuclide Target Preparation Facility. Targets were analyzed at the Lawrence Livermore National Laboratory's Center for Accelerator Mass Spectroscopy. ^{10}Be concentrations were converted to catchment-averaged erosion rates (Table I) using a constant production rate model (Lal, 1991; Stone, 2000).

Results and Interpretation

Digital elevation models (DEMs)

DEMs can be produced from classified point clouds using a number of methods. Figures 3a and 3b display NCALM bare earth and full-featured shaded relief maps made from DEMs which illustrate landscape features at 1 m resolution. The NCALM bare earth shaded-relief DEM (Figure 3a) was produced by kriging elevation values classified as bare earth with a 25 m kriging window. Even under vegetation, detailed landscape features are visible in the bare-earth DEMs. Figures 3c and 3d display IDW shaded relief DEMs produced with the online tools at http://www.opentopography.org that indicate (shown in yellow, online publication only) locations at which no laser ground returns occur within 2 m. Figure 4 displays areas in which the calculated change between 2003 and 2007 was less than ±0·25 m. The prevalence of this level of stability across the study area suggests little systematic offset between the data sets remains. That said, the mosaic pattern

Table I. Catchment averaged erosion rates from detrital ^{10}Be concentrations.

Sample	Location (deg N/ deg W)	Basin area (km^2)	Mean elevation (m)	Shielding factor	Production rate (atoms/g/yr)		Quartz (g)	Be carrier (mg)	$^{10}Be/^{9}Be$ (10^{-13})	^{10}Be concentration (10^3 atoms/g SiO_2)	Erosion rate (mm/yr)
					Spallation	Muons					
Hauser Bridge	38·5998/123·2890	85·3	294	1	5·51	0·202	109·50	0·404	0·999 ± 0·03	24·658 ± 0·65	0·232 ± 0·035
Russian Gulch	38·4712/123·3515	28·9	266	1	5·14	0·196	113·56	0·386	1·220 ± 0·03	25·494 ± 0·63	0·206 ± 0·030

across the study area does suggest random errors, and possibly returns off vegetation mapped as ground, do occasionally exceed ±0·25 m.

Change detection and volumetric flux

Figure 5 displays topographic profiles and topographic change along the A–A′ transect indicated in Figure 3d. These profiles are indicative of the high-resolution change detection that is possible using aligned, multitemporal ALSM. Figure 6 displays slope-shade maps of the Mill Gulch earthflow in 2003 and 2007. These maps are useful for making observations about changes in landscape form across the study domain. The most obvious changes include slight downslope translation of earthflow source area scarps and blocks of material, retreat of a portion of the upper headwall scarp ('A' in Figure 6), rapid translation and changes in the pattern of surface gullies ('B,C, D,E,G' in Figure 6), formation of lobes in the toe area ('F' in Figure 6) and advance and fluvial reworking of the earthflow toes onto the canyon floor at the downslope terminus of the earthflow ('H' in Figure 6). These features are mapped onto the 2003 image, and their 2003 locations are transferred onto the 2007 map to highlight changes.

Figure 7A is an elevation change map of the active earthflow and canyon-opposite slope. This change map illuminates features of the earthflow, most of which are consistent with Kelsey's (1978) detailed schematic of earthflow morphology and process derived from earthflows in Franciscan mélange along the Van Duzen River ~300 km north of this study site. These consistencies include an overall form characterized by an hourglass-shaped planform with a wide, bowl-shaped area of headscarps in the upper earthflow, a narrow transport zone in the middle reaches, and bulbous toes at the river bed (Kelsey, 1978). While the pattern of alternating surface lowering and elevation increase in the source portion of the Mill Gulch earthflow as visible on Figures 5 and 7 is mostly a result of translation of blocks of material, it is apparent that the middle transport zone was dominated by surface lowering due to movement of material from the transport zone into the toe zone. Farther downslope, the earthflow has two prominent zones of toe advance with a stable area in between. The active earthflow toe areas were dominated by surface elevation increase caused by material accumulation and thickening. The advance of the north-eastern earthflow toe into the canyon floor led to interaction with the canyon-floor channel and opposite hillslope. The channel appears to have been deflected to the east there, which led to slope failure on the opposite canyon wall, presumably caused by undermining of the slope by the canyon-floor channel. Advance of the south-western toe into the channel appears to have cause damming of the channel and local channel aggradation on the order of 2 m thick in the channel reach between the two zones of active earthflow toe advance.

Landforms that moved between ALSM scans can also be used to estimate surface velocity. These are best observed by comparing the slope shades in Figure 6, and also by inspecting the translation of steep features as mapped in Figure 7B. In the source area, distinct scarps and blocks translated between 1·5 and 2·5 m, in a fairly even pattern. In the transport region, a steep-sided gully moved ~20 m downslope with little deformation ('B' in Figure 6). In what was, evidently, a slightly slower-moving, marginal part of the transport zone, a distinct gully meander translated ~7 m downslope ('D' in Figure 6). Farther downslope in the transport region, a clearly identifiable gully meander moved ~20 m downslope ('E' in Figure 6). Even farther downslope, in the earthflow toe area, coherent movement is less visibly quantifiable, but advance of the sloped earthflow toes and

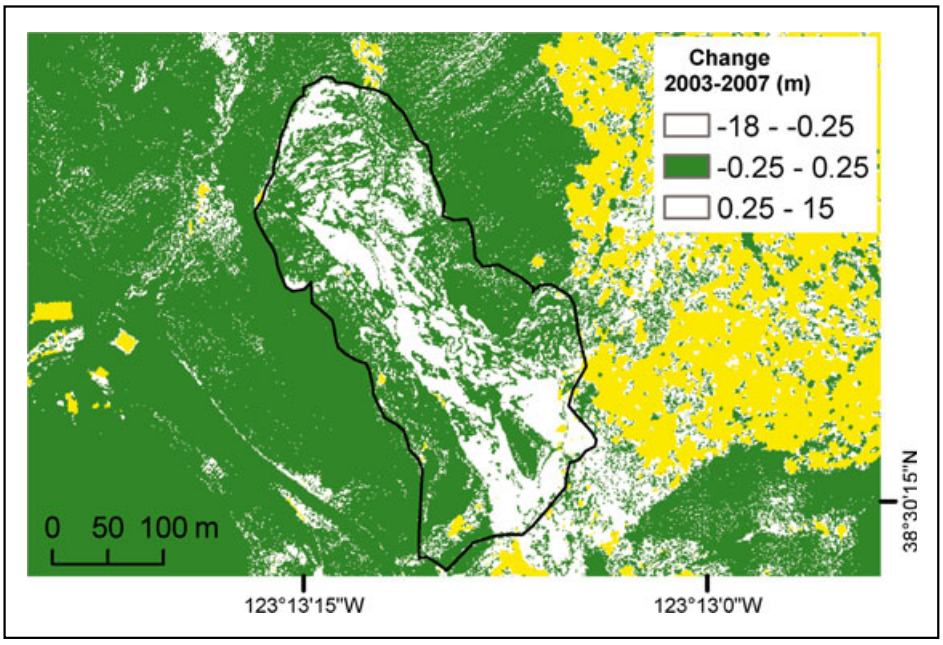

Figure 4. Map of 2003–2007 topographic change less than ±0·25 m (in green). No data is in yellow. This figure is available in colour online at wileyonlinelibrary.com/journal/espl

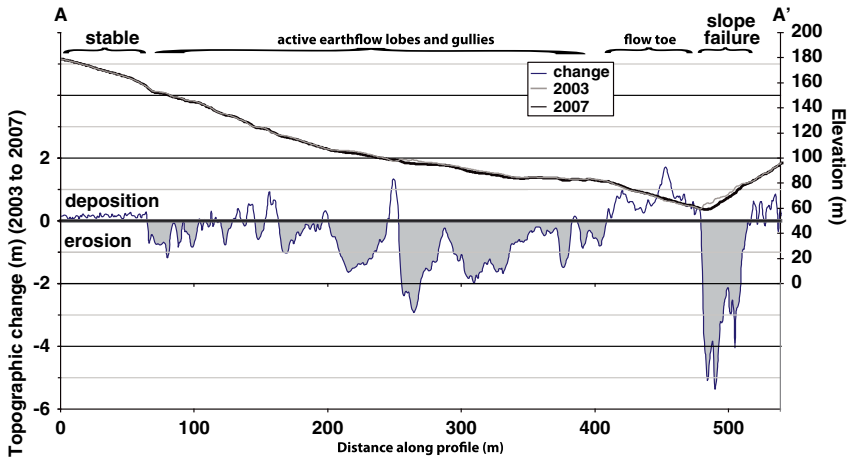

Figure 5. Topographic profiles from A–A′ (on Figure 1 d) from 2003 and 2007 data. Profile of magnitude of elevation change provided also, as are generalized process regions.

apparent thickening led to formation of a small supra-flow lobe ('F' in Figure 6), and rearrangement of gully planform geometry ('G' in Figure 6). At the downslope margin of the earthflow, interaction between lobe advance and fluvial reworking led to local change on the downstream boundary of the earthflow ('H' in Figure 6). These observations suggest a representative surface velocity of about 0·5 m/yr in the source area, and up to 5 m/yr in the transport zone.

The Mill Gulch earthflow headwall is at the ridge-top divide along a portion of its length, limiting incorporation of new material into the flow. Only the northern edge of the earthflow headwall has any stable upslope area to incorporate into the flow, and it only eroded headward in one small, distinct area (at 'A' in Figure 6). The transport zone is moving material more rapidly that has been replenished, leading to surface lowering. This material has accumulated in the toe zone, where it will be susceptible to future evacuation by floods. The accumulation of material in the earthflow toes should buffer significant fluvial incision by supplying significant alluvial bed cover, and the lack of upstream area for the earthflow to incorporate may lead to a decline in earthflow activity at Mill Gulch in the coming decades, unless it advances further to the north.

Histograms of erosion and deposition were generated following methods presented in Wheaton *et al.* (2010) (Figure 8). These allow for calculation of the net volumetric loss of the Mill Gulch earthflow and opposite-slope failure. Taking into account all pixels in the area of analysis, the volumetric loss is 3693 m^3. Using the conservative assumption that there is scatter of ±0·25 m around the zero change value due to random elevation errors (this value was chosen based on data collection specifications and the amplitude of noise in the topographic profile in Figure 2a), and disregarding all pixels with change 0·25 m, the volumetric loss is 3832 m^3. The similarity of these two volumetric change values further suggests these alignment methods are robust because it indicates the least-changing regions have change magnitudes that are nearly symmetrical about zero.

Using 3800 m^3 as the net volume loss over four years and assuming no density changes, the erosion rate is 14·0 ± 1 mm/yr across the 0·066 km^2 analysis area, which consists of the earthflow itself and the opposite canyon slope where it failed between ALSM scans. Assuming earthflow material has a density similar to colluvium of 2·1 g/cm^3 the sediment yield is 30 000 t/ km^2/yr, from the Mill Gulch earthflow. This is higher than

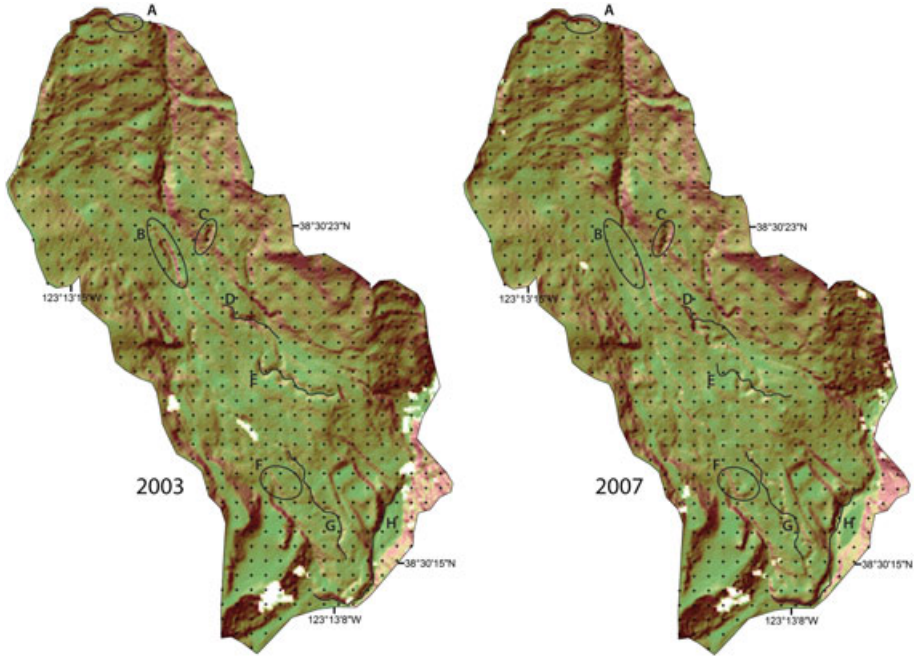

Figure 6. Slope-shade maps (slope is colored from green to red linearly from 0 to 90º as slope increases, and is layered transparently onto a shaded relief map) of the Mill Gulch earthflow in 2003 and 2007. Tick marks are separated by 10 m. Several zones of distinct process are mapped onto the 2003 map, and those locations are transferred onto the 2007 map to illustrate change: A, earthflow headwall retreat; B, prominent steep-sided gully; C, gully; D and E, meandering gullies; F, zone of flow lobe development; G, meandering gully; H, margin of flow in canyon floor. This figure is available in colour online at wileyonlinelibrary.com/journal/espl

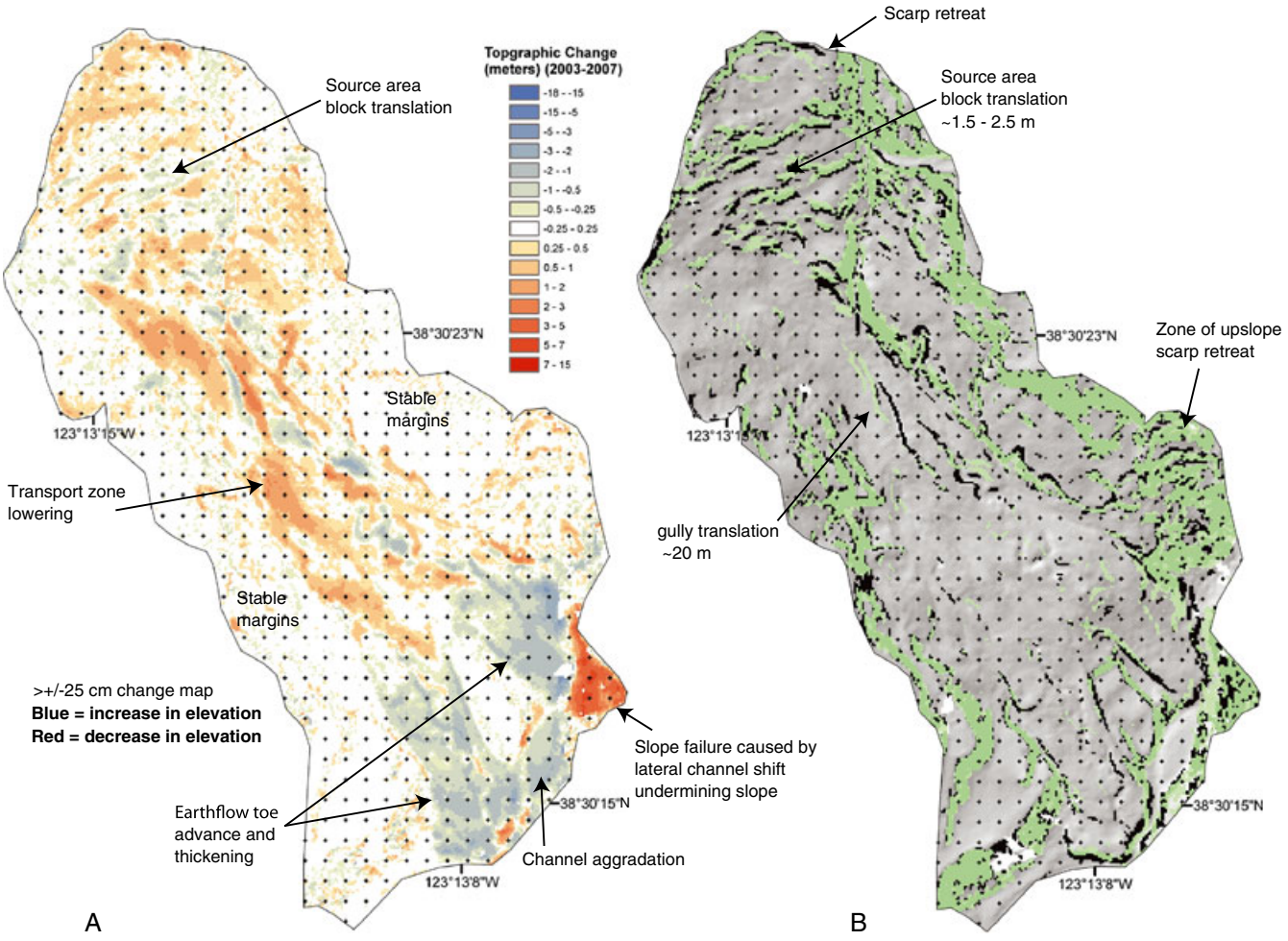

Figure 7. (A) Map of elevation changes between 2003 and 2007. Blue indicates elevation increase, and red indicates elevation decrease. Notation highlights several zones of distinct change or stability. (B) Map of steep (> 28° profile steepness) zones in 2003 (green) and 2007 (black) to display downslope translation of distinct landforms as well as upslope-directed scarp retreat. This figure is available in colour online at wileyonlinelibrary.com/journal/espl

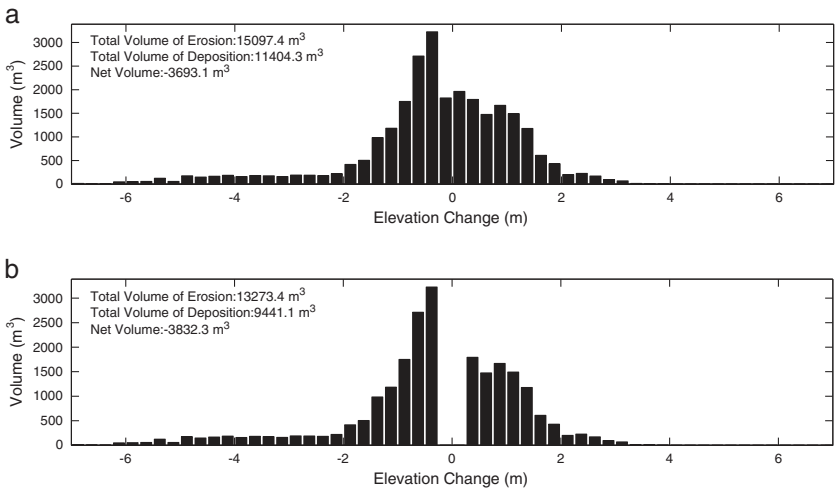

Figure 8. Histograms of distribution of erosion and deposition on the Mill Gulch earthflow. (a) All pixels used. (b) Only pixels with > 0·25 m change used.

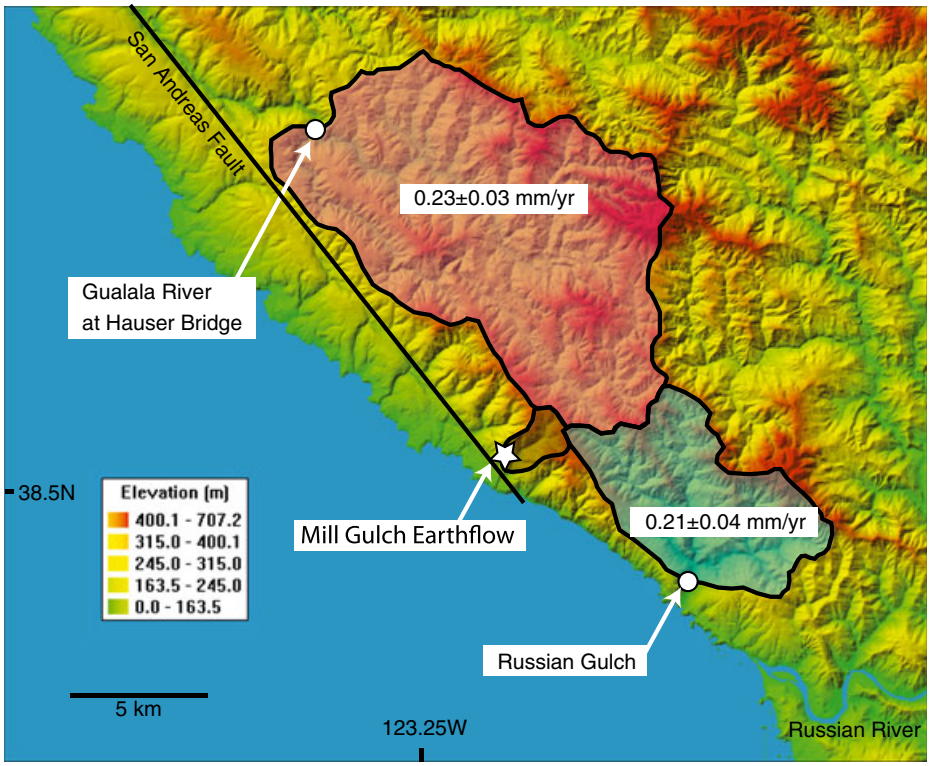

Figure 9. Catchment-averaged millennial-scale erosion rates as determined by CRN concentrations in fluvial sediment. Catchments are mapped onto shaded relief map, including the catchment that contains the Mill Gulch earthflow. This figure is available in colour online at wileyonlinelibrary.com/journal/espl

24 900 t/km^2/yr reported by Kelsey (1978), and 19 000 t/km^2/yr reported by Mackey and Roering (2011), who averaged sediment delivery from many earthflows. This local sediment delivery rate is, unsurprisingly, far higher than previously reported catchment-averaged erosion rates elsewhere in coastal northern California that integrate areas of mass movement with far more stable areas of the landscape. These include ~0·1–0·15 mm/yr from cosmogenic radionuclide (CRN) concentrations in fluvial sediments at Tennessee Valley ~100 km south (O'Farrell *et al.*, 2007) and ~0·09–0·4 mm/yr from CRNs at Caspar and Redwood Creeks ~300 km north of the study area (Ferrier *et al.*, 2005), 0·9 mm/yr from suspended sediment load at the Scotia gauging station on the Eel River ~400 km north of Mill Gulch (Wheatcroft and Sommerfield, 2005), and 0·16–0·22 mm/yr from modern alluvium in the Eel River drainage basin (Fuller *et al.*, 2009). Assuming erosion on the Mill Gulch earthflow is the dominant erosion process in the entire ~2·8 km^2 Mill Gulch catchment, the full catchment averaged erosion rate is ~0·30 mm/yr. This rate, when compared to the nearby estimates, agrees at an order-of magnitude level, but is somewhat higher reflecting the dominance of the single large area of active mass wasting at the Mill Gulch earthflow within the relatively small catchment area. Furthermore, this is obviously a minimum erosion rate because erosion was likely to have occurred elsewhere in the catchment in areas covered by dense vegetation or outside the area of ALSM mapping and therefore not in our analysis area during the studied time interval.

Annual-scale, catchment-averaged minimum erosion rate determined from ALSM change detection can now be compared to longer-term catchment averaged erosion rates derived

from CRN concentrations in fluvial sediment from adjacent watersheds. CRN-derived catchment-averaged erosion rates from fluvial sediments at the Gualala River at Hauser Bridge, and Russian Gulch are $0{\cdot}23 \pm 0{\cdot}03$ and $0{\cdot}21 \pm 0{\cdot}04$ mm/yr, respectively (Figure 9). These rates are in order-of-magnitude agreement with the ALSM-derived erosion rates; though represent an average rate over much larger drainage basins on much longer timescales. The higher rates from the Mill Gulch earthflow may indicate that earthflows deliver large amounts of sediment over short periods of time but their effects are somewhat diminished when averaged over longer time intervals and larger areas (e.g. Kelsey, 1978). The Mill Gulch earthflow covers 2·4% of the area of the Mill Gulch catchment. Mackey and Roering (2011) documented that earthflows covering 6% of their Eel River study area supply half of the channel sediment load over a period of several decades. This may suggest the Mill Gulch earthflow was particularly active during the period 2003–2007, in comparison to the average earthflow formed in Franciscan Complex in northern California, especially when measured over longer timescales. Earthflow activity can almost certainly intermittently raise a catchment sediment delivery rate so catchment fluvial sediment transport monitoring in earthflow-prone terrains must take into account the short-term rate of activities on earthflows in order to properly understand multi-year catchment sediment production.

One way to evaluate these hypotheses would be to establish erosion rate monitoring using multitemporal ALSM mapping across catchments over many years coupled with measurements of channel sediment flux and long-term erosion rate measurements from CRNs. This requires ongoing commitment to collecting baseline ALSM data, and an effort to collect multitemporal ALSM as well as rapid response ASLM mapping after significant landscape altering events such as storms and large earthquakes.

Conclusions

Gridded multitemporal ALSM data can be used for change detection to the sub-meter level if properly aligned. The rigorous alignment of disparate datasets is essential if the magnitude of landscape change is to be calculated, though the spatial distribution of erosion and deposition will be less sensitive to this. Widely available bare-earth DEMs should be used cautiously in vegetated areas. DEMs should be generated conservatively by querying the classified point cloud using limited search radius algorithms, in order to avoid attempting sub-meter change detection in areas with dense vegetation canopy. Higher resolution change could also be calculated by aligning point cloud datasets in lieu of raster datasets, requiring more sophisticated processing.

At Mill Gulch in northern California multitemporal ALSM reveals subtle changes on an earthflow formed in Coastal Belt Franciscan Complex (Bailey *et al*, 1964). The most significant changes were translation of blocks of material 1–3 m within the earthflow source area, translation of material up to 20 m in the middle transport reach with accompanying 0–2 m of surface lowering, and an accumulation and thickening of material in the earthflow toe of 2–3 m. The earthflow appears to have partially dammed the canyon-floor channel causing increased sediment storage in the channel and forcing the channel to migrate laterally which caused a significant sloe failure opposite the earthflow. The spatial patterns of these changes are mapped at meter-scale horizontal, and centimeter-scale vertical resolution.

The total volume lost by this earthflow was ~3800 m^3 over the four year period. This is equivalent to a catchment-averaged erosion rate of ~0·3 mm/yr across the entire Mill Gulch watershed, which is only slightly higher than millennial scale erosion rates from two adjacent watersheds, indicating that earthflows can contribute significant volumes of sediment to a watershed sediment budget over short timescales. Multitemporal ALSM change detection holds great promise for high precision landscape change detection performed remotely over large spatial scales. We encourage further baseline data acquisition and planning for rapid post-event data acquisition, particularly in areas susceptible to earthquakes and mass movements.

Acknowledgments—SBD was supported by a US Geological Survey Mendenhall Postdoctoral Research Fellowship. Thanks to N. Glenn and C. Crosby for helpful conversations, and to J. Wheaton and an anonymous reviewer for helpful review.

References

Arrowsmith JR, Zielke O. 2009. Tectonic geomorphology of the San Andreas Fault Zone from high resolution topography: an example from the cholame segment. *Geomorphology* **113**: 70–81.

Bailey EH, Irwin WP, Jones DL. 1964. Franciscan and related rocks. *California Division of Mines and Geology Bulletin* **183**: 177.

Baldo M, Bicocchi C, Chiocchini U, Giordan D, Lollino G. 2009. LIDAR monitoring of mass wasting processes: the Radicofani landslide, Province of Siena, central Italy. *Geomorphology* **105**(3–4): 193–201. DOI. 10.1016/j.geomorph.2008.09.015

Baum RL, Messerich J, Fleming RW. 1998. Surface deformation as a guide to kinematics and three-dimensional shape of slow-moving, clay-rich landslides, Honolulu, Hawaii. *Environmental and Engineering Geoscience* **4**: 283–306.

Bull JM, Miller H, Gravley DM, Costello D, Hikuroa DCH, Dix JK. 2010. Assessing debris flows using LIDAR differencing: 18 May 2005 Matata event, New Zealand. *Geomorphology* **124**(1–2): 75–84.

Bulmer MH, Petley DN, Murphy W, Mantovani F. 2006. Detecting slope deformation using two-pass differential interferometry: implications for landslide studies on Earth and other planetary bodies. *Journal of Geophysical Research* **111**: E06S16. DOI. 10.1029/2005JE002593

Burns WJ, Coe JA, Kaya BS, Ma L. 2010. Analysis of elevation changes detected from multi-temporal LiDAR surveys in forested landslide terrain in western Oregon. *Environmental and Engineering Geoscience* **26**(4): 315–341. DOI. 10.2113/gseegeosci.16.4.315

Coe JA, McKenna JP, Godt JW, Baum RL. 2009. Basal-topographic control of stationary ponds on a continuously moving landslide. *Earth Surface Processes and Landforms* **34**(2): 264–279. DOI. 10.1002/esp.1721

Corsini A, Borgatti L, Cervi F, Dahne A, Ronchetti F, Sterzai P. 2009. Estimating mass-wasting processes in active earth slides – earth flows with time-series of high-resolution DEMs from photogrammetry and airborne LiDAR. *Natural Hazards and Earth System Sciences* **9**: 433–439. DOI. 10.5194/nhess-9-433-2009

Corsini A, Borgatti L, Coren F, Vellico M. 2007. Use of multitemporal airborne lidar surveys to analyse post-failure behaviour of earth slides. *Canadian Journal of Remote Sensing* **33**: 116–120. DOI. 10.5589/m07-015

Delacourt C, Allemand P, Berthier E, Raucoules D, Casson B, Grandjean P, Pambrun C, Varel E. 2007. Remote-sensing techniques for analysing landslide kinematics; a review (in issues in landslide process monitoring and understanding). *Bulletin de la Societe Geologique de France* **178**(2): 89–100. DOI. 10.2113/gssgfbull.178.2.89

DiBiase RA, Whipple KX, Heimsath AM, Ouimet WB. 2010. Landscape form and millennial erosion rates in the San Gabriel Mountains, CA. *Earth and Planetary Science Letters* **289**: 134–144.

Ferrier KL, Kirchner JW, Finkel RC. 2005. Erosion rates over millennial and decadal timescales at Caspar Creek and Redwood Creek, northern California Coast Ranges. *Earth Surface Processes and Landforms* **30**: 1025–1038. DOI. 10.1002/esp.1260

Fuller TK, Perg LA, Willenbring JK, Lepper K. 2009. Field evidence for climate-driven changes in sediment supply leading to strath terrace formation. *Geology* **37**: 467–470. DOI. 10.1130/G25487A.1

Glenn NF, Streutker DR, Chadwick J, Thackray GD, Dorsch S. 2006. Analysis of LiDAR-derived topographic information for characterizing

and differentiating landslide morphology and activity. *Geomorphology* **73**: 131–148.

Hilley GE, Bürgmann R, Ferretti A, Novali F, Rocca F. 2004. Dynamics of slow-moving landslides from permanent scatterer analysis. *Science* **304**: 1952–1954.

Houser C, Hapke C, Hamilton S. 2008. Controls on coastal dune morphology, shoreline erosion and barrier island response to extreme storms. *Geomorphology* **100**(3–4): 223–240. DOI. 10.1016/j.geomorph.2007.12.007

Iverson RM, Major JJ. 1987. Rainfall, groundwater flow, and seasonal movement at Minor Creek landslide, northwestern California: physical interpretation of empirical relations. *Geological Society of America Bulletin* **99**: 579 594.

Jaboyedoff M, Oppikofer T, Abellán A, Derron M, Loye A, Metzger R, Pedrazzini A. 2010. Use of LIDAR in landslide investigations: a review. *Natural Hazards* **1**: 24. DOI. 10.1007/s11069-010-9634-2

Keefer DK, Johnson AM. 1983. Earth Flows: Morphology, Mobilization, and Movement, US Geological Survey Professional Paper 1264. US Geological Survey: Reston, VA.

Kelsey HM. 1978. Earthflows in Franciscan melange, Van Duzen River basin, California. *Geology* **6**: 361–364.

Lal D. 1991. Cosmic ray labeling of erosion surfaces: in situ nuclide production rates and erosion models. *Earth and Planetary Science Letters* **104**: 424–439.

Lazarus ED, Murray AB. 2007. Process signatures in regional patterns of shoreline change on annual to decadal time scales. *Geophysical Research Letters* **34**: L19402. DOI. 10.1029/2007GL031047

Mackey BH, Roering JJ. 2011. Sediment yield, spatial characteristics, and the long-term evolution of active earthflows determined from airborne LiDAR and historical aerial photographs, Eel River, California. *Geological Society of America Bulletin*. DOI. 10.1130/B30306.1.1

Mackey B, Roering J, McKean J. 2009. Long-term kinematics and sediment flux of an active earthflow, Eel River, California. *Geology* **37**: 803–806.

Malet J-P, Maquaire O, Calais E. 2002. The use of global positioning system techniques for the continuous monitoring of landslides: application to the Super-Sauze earthflow (Alpes-de-Haute-Provence, France). *Geomorphology* **43**(1–2): 33– 54.

Manson MW, Huyette CM, Wills CJ, Huffman ME, Smelser MG, Fuller ME, Domrose C, Gutierrez C. 2006. *Special Report 196 – Landslides in the Highway 1 Corridor between Bodega Bay and Fort Ross, Sonoma County, California*. California Geological Survey: Sacramento, CA; 26.

Merritts D, Hilley GH, Arrowsmith JR, Carter B, Dietrich W, Jacobs J, Martel S, Roering J, Shrestha R, Snyder N. 2008. Report to the National Science Foundation: Workshop on Studying Earth Surface Processes with High Resolution Topographic Data. http://pages.uoregon.edu/jroering/outgoing/LiDAR_Workshop_White_Paper_Final_2008.pdf (accessed April 19, 2011).

Mitasova H, Overton MF, Recalde JJ, Bernstein DJ, Freeman CW. 2009. Raster-based analysis of coastal terrain dynamics from multitemporal LiDAR data. *Journal of Coastal Research* **25**(2): 507–514.

National Center for Airborne Laser Mapping (NCALM). 2007. Northern California Fault System LiDAR Survey Metadata. http://opentopo.sdsc.edu/metadata/NoCAL_REPORT_8-11-09_FINAL_ii.pdf (accessed April 14, 2011).

O'Farrell CR, Heimsath AM, Kaste JM. 2007. Quantifying hillslope erosion rates and processes for a coastal California landscape over varying timescales. *Earth Surface Processes and Landforms* **32**: 544–560.

Pelletier JD, Mitasova H, Harmon RS, Overton M. 2009. The effects of interdune vegetation changes on eolian dune field evolution: a numerical-modeling case study at Jockey's Ridge, North Carolina, USA. *Earth Surface Processes and Landforms* **34**(9): 1245–1254. DOI. 10.1002/esp.1809

Roering JJ, Stimely LL, Mackey BH, Schmidt DA. 2009. Using DInSAR, airborne LiDAR, and archival air photos to quantify landsliding and sediment transport. *Geophysical Research Letters* **36**: L19402. DOI. 10.1029/2009GL040374

Soler T, Snay RA. 2003. Transforming positions and velocities between the International Terrestrial Reference Frame of 2000 and North American Datum of 1983. *Journal of Survey Engineering* **130**: 2. DOI. 10.1061/(ASCE)0733-9453(2004)130:2(49)

Stone JO. 2000. Air pressure and cosmogenic isotope production. *Journal of Geophysical Research* **105**(23): 753–759.

Streutker DR, Glenn NF, Shrestha R. 2011. A slope-based method for matching elevation surfaces. *Photogrammetric Engineering and Remote Sensing* **77**(7): 743– 750.

Strozzi T, Farina P, Corsini A, Ambrosi C, Thüring M, Zilger J, Wiesmann A, Wegmüller U, Werner C. 2005. Survey and monitoring of landslide displacements by means of L-band satellite SAR interferometry. *Landslides* **2**(3): 193–201. DOI. 10.1007/s10346-005-0003-2

TerraPoint LLC, Harding D. 2004. Northern San Andreas Fault, CA and West Rainier Seismic Zone, WA LiDAR Metadata Report. http://opentopo.sdsc.edu/metadata/NSAF_Rainier_LiDAR_metadata.pdf

Tarolli P, Arrowsmith JR, Vivoni ER. 2009. Understanding earth surface processes from remotely sensed digital terrain models. *Geomorphology* **113**: 1–3. DOI. 10.1016/j.geomorph.2009.07.005

Woolard JW, Colby JD. 2002. Spatial characterization, resolution, and volumetric change of coastal dunes using airborne LIDAR: Cape Hatteras, North Carolina. *Geomorphology* **48**(1–3): 269–287. DOI. 10.1016/S0169-555X(02)00185-X

Wheatcroft RA, Sommerfield CK. 2005. River sediment flux and shelf sediment accumulation rates on the Pacific Northwest margin. *Continental Shelf Research* **25**: 311–332.

Wheaton JM, Brasington J, Darby SE, Sear D. 2010. Accounting for uncertainty in DEMs from repeat topographic surveys: improved sediment budgets. *Earth Surface Processes and Landforms* **35**(2): 136–156. DOI. 10.1002/esp.1886

Zhou G, Xie M. 2009. Coastal 3-D morphological change analysis using LiDAR series data: a case study of Assateague Island national seashore. *Journal of Coastal Research* **25**(2): 435–447.